Ultramicroscopy 123 (2012) 28–37

Contents lists available at SciVerse ScienceDirect

Ultramicroscopy

journal homepage: www.elsevier.com/locate/ultramic

Seeing the atoms more clearly: STEM imaging from the Crewe era to today

S.J. Pennycook*

Oak Ridge National Laboratory, Materials Science and Technology Division, PO Box 2008, Oak Ridge, TN 37831-6071, United States

ARTICLE INFO

Available online 5 June 2012

Keywords:
Scanning transmission electron microscopy
Electron energy loss spectroscopy
Aberration correction
Z-contrast
Atomic resolution

ABSTRACT

This review covers the development of scanning transmission electron microscopy from the innovations of Albert Crewe to the two-dimensional spectrum imaging in the era of aberration correction. It traces the key events along the path, the first atomic resolution Z-contrast imaging of individual atoms, the realization of incoherent imaging in crystals and the role of dynamical diffraction, simultaneous, atomic resolution electron energy loss spectroscopy, and finally the tremendous impact of the successful correction of lens aberrations, not just in terms of resolution but also in single atom sensitivity.

© 2012 Elsevier B.V. All rights reserved.

1. The Crewe era

Albert Crewe and his coworkers laid the foundations for the modern-day scanning transmission electron microscope (STEM), with their realization that brightness is everything. Their use of a cold field emission source and an annular detector produced the first atomic-resolution images of single atoms and the first simultaneous electron energy loss spectroscopy (EELS). This review traces these and subsequent developments that have led to the development of modern aberration corrected instruments, bringing sub-Angstrom resolution, the imaging of individual light atoms, and two-dimensional atomic-resolution spectroscopic imaging. This is a succinct version of a much longer historical account of the development of STEM that was published recently [1].

Although Crewe is thought of as the father of STEM, it was actually conceived not long after the development of the first TEM by Knoll and Ruska [2]. Baron Manfred von Ardenne [3,4] developed the STEM, placing the imaging lens before the specimen instead of after the specimen as in the Ruska TEM design. He realized that the transmitted electrons would not need to be focused to form a high resolution image, merely detected, and so the STEM optics would avoid any chromatic aberration due to energy losses suffered during transmission through the specimen. While this was a sound idea in principle, he did not use a field emission source, and although he achieved a resolution of 10 nm the images were very noisy. He quickly abandoned the STEM in favor of the Ruska-style TEM design [5,6].

Almost 30 years pass before the STEM is taken up again by Crewe, who realized the necessity of using a high brightness cold field emission gun [7] to achieve sufficient beam current in a small probe. The first machine produced a resolution of 30 Å [8]. Over the next few years a new design produced a resolution stated to be about 5 Å, [9,10] but was actually closer to 2.5 Å (see [11]). This resolution allowed the first imaging of individual atoms in an electron microscope, using molecules stained with uranium and thorium atoms. The images were formed from the ratio of the elastic signal collected by the annular detector to the inelastic signal collected by the spectrometer. The cross section ratio is approximately proportional to atomic number Z and so they called the ratio image a "Z-contrast" image [12]. Wall et al., [13] showed line traces of the annular detector signal across individual atoms demonstrating unequivocally a probe size of 2.5 Å, and also images of small crystallites, as shown in Fig. 1.

With this microscope phase contrast images were also obtained by using a small axial collector aperture [9]. The images were similar to those obtained with a small axial condenser aperture of the TEM, thus demonstrating the principle of reciprocity [14,15]. Significant effort was also put into the development of EELS, which revealed its great promise as a microanalytical technique [16], spurring the development of modern analytical electron microscopy.

2. Z-contrast for materials science

The spectacular results generated by the Crewe group led to the establishment of the first commercial manufacturer of a dedicated STEM, VG Microscopes [17], and the emergence of the STEM as a high resolution analytical microscope [18]. Materials, however, unlike the biological systems of primary interest to the Crewe group, are typically crystalline, with strong diffraction effects. Attempts to use the Crewe ratio method for Z-contrast imaging were unsatisfactory because diffraction contrast tended

* Tel.: +865 574 5504; fax: +865 574 6098.
E-mail address: pennycooksj@ornl.gov

0304-3991/$ - see front matter © 2012 Elsevier B.V. All rights reserved.
http://dx.doi.org/10.1016/j.ultramic.2012.05.005

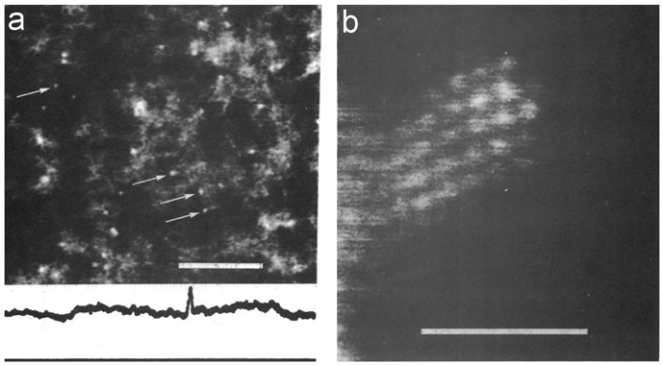

Fig. 1. (a) Annular dark field (ADF) image of a sample of mercuric acetate showing individual atoms obtained with the Crewe STEM. The line trace across a single atom shows a full width half maximum of 2.5 ± 0.2 Å. Scale bar is 50 Å. (b) ADF image of small crystallites containing uranium and thorium atoms. Scale bar is 20 Å. Reproduced from Ref. [13] with permission.

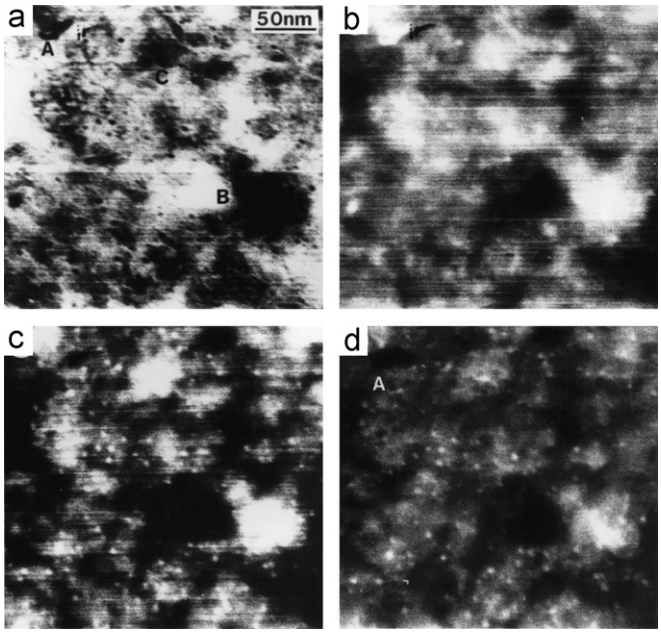

Fig. 2. Images of Pt particles on γ-alumina recorded in (a) bright field, (b) low angle ADF, (c) HAADF and (d) the ratio of high angle to low angle ADF signals. Particle contrast is highest in the HAADF image, reproduced from M.M.J. Treacy, PhD thesis, University of Cambridge, 1979, with permission.

to dominate any Z-contrast that might be present, making interpretation ambiguous [19]. More success was had imaging catalyst particles [20], leading to the idea of a high angle annular dark field (HAADF) detector where coherent diffracted beams would be replaced by thermal diffuse scattering, otherwise known as Rutherford scattering, with a scattering cross section approaching Z^2 [21]. Such a signal should therefore give enhanced Z-contrast compared to the Crewe ratio method, with minimal diffraction effects. The idea was tested by [22], and a comparison with the bright field, Crewe-style wide angle annular detector and a ratio image is shown in Fig. 2. The HAADF image shows the best contrast.

The technique was used to image dopant profiles in ion-implanted single crystal Si, where the suppression of diffraction contrast in the HAADF signal is quite apparent, see Fig. 3 [23]. Such results naturally led to the question of the ultimate resolution of the Z-contrast signal in a crystalline material. Clearly, if the crystal were a monolayer raft of atoms then atomic resolution would be expected with a sufficiently small probe, like in the

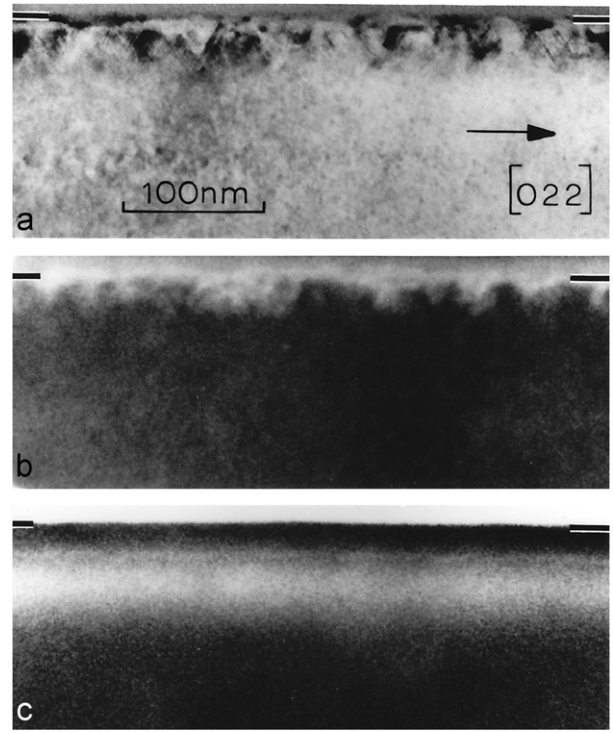

Fig. 3. Cross section images of Sb implanted Si. (a) TEM diffraction contrast image showing defects near the surface and end of range damage, (b) Low angle ADF image also dominated by diffraction contrast, (c) HAADF image revealing the Sb distribution. Reproduced from Ref. [23].

Crewe images. And since Rutherford scattering is at high angles, it is generated close to the nucleus of each atom, and each atom can be considered an independent source. The situation is precisely analogous to the self-luminous source in light optics which produces an incoherent image [24]. An incoherent image shows no contrast reversals as focus is changed, like the image in a camera, and also shows better resolution than a coherent phase contrast image, as was appreciated by the Crewe group. However, the role of dynamical diffraction in thicker crystals was not known. Cowley [25] actually published an image demonstrating the improved resolution of the ADF image over the bright field phase contrast image, but surprisingly made no mention of any incoherent characteristics associated with the ADF image. Incoherent characteristics had been predicted theoretically for single atoms by Engel [26] and for weak phase objects by Misell [27], but the issue was controversial for high resolution [28] and for atoms in a column [29].

Incoherent characteristics were observed in HAADF images from crystals of the high temperature superconductors $YBa_2Cu_3O_{7-\delta}$ and $PrBa_2Cu_3O_{7-\delta}$, using a VG Microscopes HB501UX with a high resolution pole piece producing a theoretical probe size of 0.22 nm [30,31]. The contrast showed the expected dependence on atomic number and freedom from contrast reversals with thickness and objective lens focus. Fig. 4 shows images of the semiconductors Si and InP viewed along the $\langle 110 \rangle$ zone axis [32]. In this orientation the atoms form closely spaced pairs of columns referred to as dumbbells. Although the Si dumbbells spaced 0.136 nm apart are not resolved, they are clearly elongated, indicating the presence of the two columns. In the case of the InP the high Z of the In column dominates the image contrast and circular features are seen instead. Besides the lack of contrast reversals, a more surprising result was the apparent lack of any evidence of dynamical diffraction with increasing specimen thickness, the image intensity simply rising with increasing sample

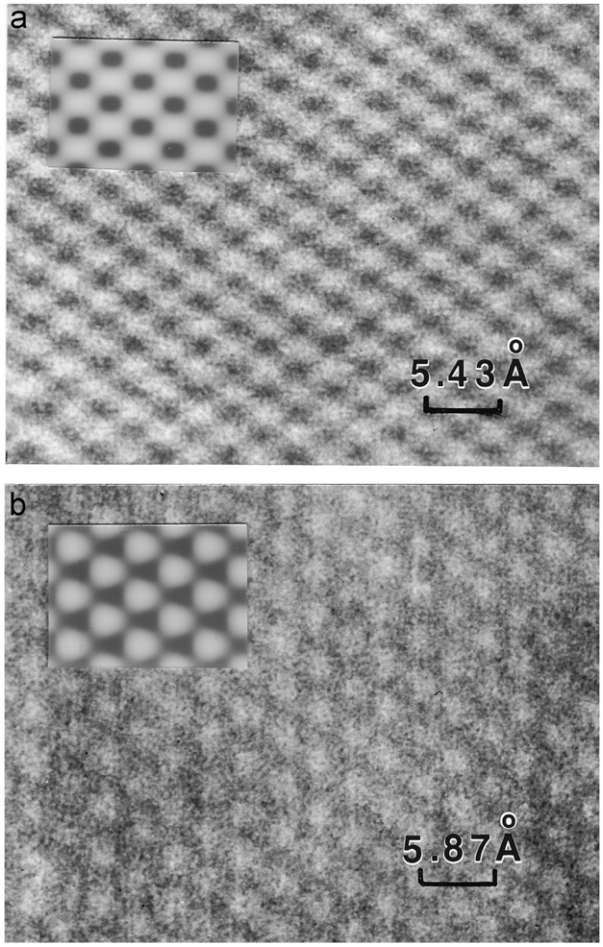

Fig. 4. Z-contrast images from (a) Si and (b) InP in the ⟨110⟩ zone axis showing how the elongated features characteristic of the Si dumbbells are absent from InP where the image is dominated by the heavy In column. Insets show simulated images, reproduced from Ref. [32].

thickness, while at the same time the bright field image showed the usual thickness fringes [33].

A physical explanation for this behavior came through an analysis of the important Bloch waves contributing to the images. While the thickness fringes in the usual phase contrast images are due to the interference between Bloch states [34], for high angle scattering the 1s state is much more important than any other, since it is the state that peaks strongly at the atomic sites where the Rutherford scattering is generated. Hence, the interference effects are strongly suppressed [32,33]. More detailed studies showed the role of the large angular range of the detector in destroying coherence between columns [35] and the need for phonons to destroy correlations along the columns [36]. The frozen phonon method for image simulation demonstrated quantitative agreement between full image simulations and the incoherent imaging model [37].

Z-contrast images of interfaces [38–40] were revealing structures that had not been expected, illustrating the power of the incoherent image for direct interpretation. It was therefore natural to move to a higher accelerating voltage to improve the spatial resolution. Fig. 5 shows images of Si and GaAs taken using a 300 kV STEM with theoretical probe size of 0.13 nm, sufficient to resolve the dumbbells, and in the case of the compound semiconductor to reveal the sublattice polarity directly in the image [41–44]. This capability offered insights into the core structures of dislocations [45,46], and allowed images of single Pt atoms and clusters to be obtained on a real catalyst support

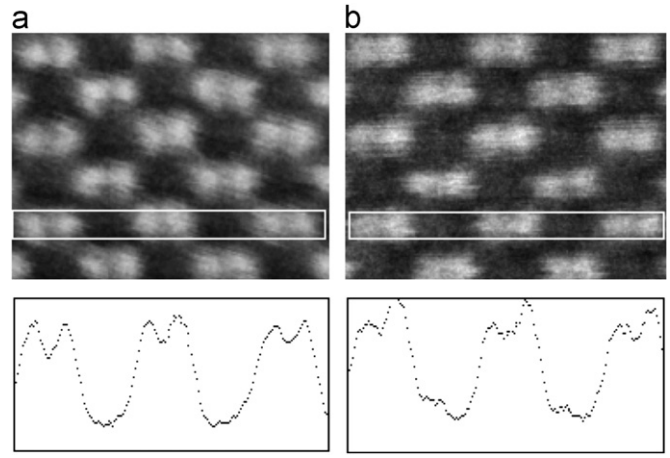

Fig. 5. Sublattice sensitivity in a 300 kV VG Microscopes HB603U STEM. Z-contrast images of (a) Si and (b) GaAs ⟨110⟩ with line traces averaged vertically within the white rectangles, adapted from Ref. [44].

[47]. Insights were obtained into grain boundary structure [48–50] including the role of impurities [51], and individual impurity sites could even be observed for the first time [52,53].

3. Atomic resolution EELS

Crewe's first microscope had no annular detector; it had a spectrometer to allow imaging at zero loss or at a chosen value of energy loss. He felt that the EELS signal held the greatest promise for high contrast [8] since it contained much information, and it should be possible to use all the electrons that lose energy. Indeed, the common DNA bases could be easily distinguished in the low loss region of the spectrum [54]. The simultaneous detection of elastic scattering with an ADF detector and inelastic scattering with the spectrometer was a feature incorporated into their next microscope, and was used to form images of single atoms as described previously. It was therefore a natural extension to attempt atomic resolution EELS in a crystal using the HAADF image to locate the beam over a specific column or plane of atoms. A Si(111)/$CoSi_2$ interface was used for the experiment since such interfaces were atomically abrupt over extended areas. A high sensitivity parallel detection system [55] was used to collect spectra plane by plane across the interface as shown in Fig. 6 (see also [56]), and the Co L edge practically disappears on moving the beam from the last Co plane to the first plane of the Si [57–59]. The same year, column by column spectroscopy was shown at a Si(100)/SiO_2 interface [60] along with sub-nm resolution imaging of core loss fine structure [61]. Column by column detection of impurity concentration and valence was demonstrated at a Mn-doped $SrTiO_3$ grain boundary [62]. Numerous applications followed to a wide range of materials [53,63–68] and the spectrum imaging technique was introduced [69,70]. Interfaces in transition metal oxides are particularly suited to study by EELS because of the wealth of information available in the fine structure [71–74], both at the transition metal L-edges and at the O K edge [75–78].

4. Aberration correction

Following the first proposals for aberration correction by Scherzer [80], the principles have been developed over many decades, see the accounts in [81–83], including notable contributions from the Crewe group [84–87]. However, successful technological implementation

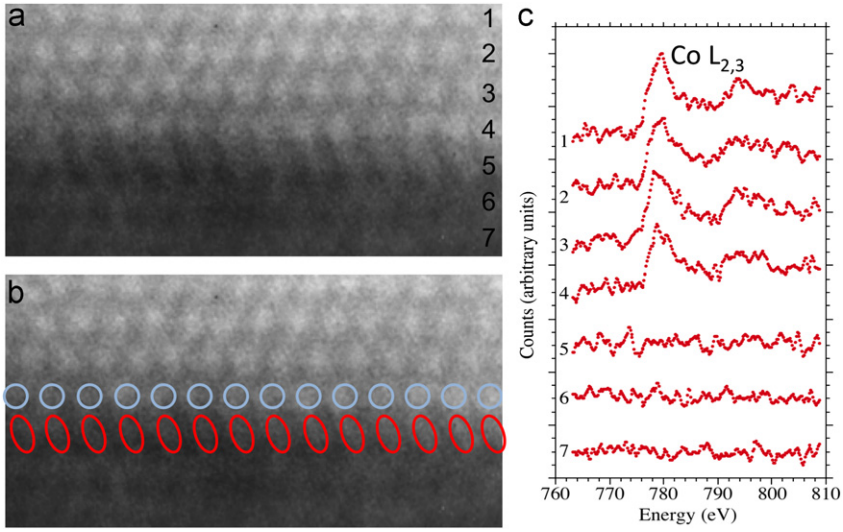

Fig. 6. (a) Z-contrast image of a $CoSi_2$/Si {111} interface showing Co columns as circles and Si dumbbells as ovals. These characteristic shapes show the interface to be atomically abrupt (b). (c) Spectra obtained plane by plane across the interface demonstrating atomic resolution spectroscopy. Spectra 1–4 were background subtracted by the usual power law fit, spectra 5–6 were obtained using the spatial difference method [79], using a reference spectrum from Si far from the interface. Data obtained with a VG Microscopes HB501UX, adapted from Refs. [57–59].

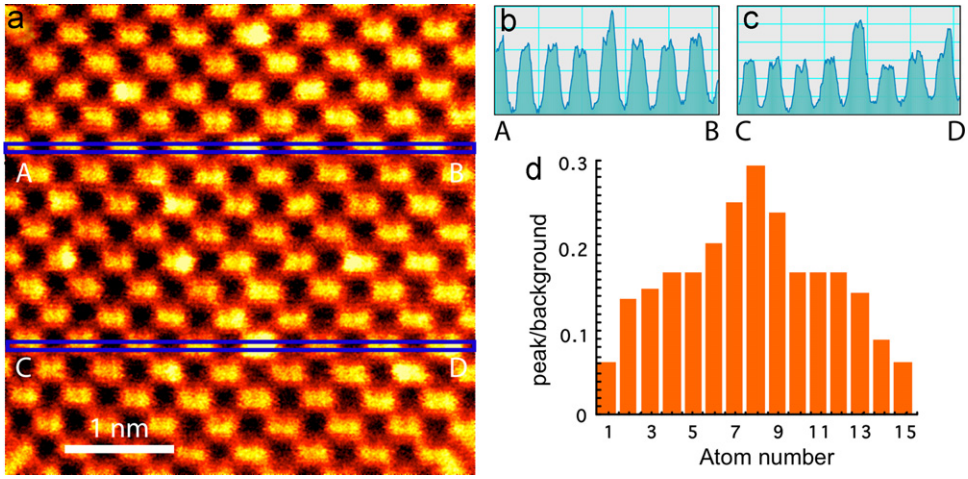

Fig. 7. (a) Z-contrast image of Bi-doped Si ⟨110⟩ taken with a VG Microscopes HB501UX with Nion aberration corrector operating at 100 kV, revealing columns containing individual Bi atoms. (b) Intensity profile along line AB shows a Bi atom on the right hand column of a Si dumbbell. (c) Profile along line CD shows a Bi atom in each of the two columns of a dumbbell. (d) Histogram of Bi atom intensities. Reproduced from Ref. [91].

had to wait until the development of fast computers and sensitive charge-coupled-device detectors to achieve the necessary precision.

The successful correction of aberrations was first demonstrated in the TEM using a hexapole corrector [88] and in the STEM using a quadrupole/octupole corrector [89]. After some improvements, resolution of the dumbbells in Si ⟨110⟩ at 1.36 Å was achieved at an accelerating voltage of only 100 kV [90]. Fig. 7 shows individual Bi atoms visible as bright spots within specific Si columns [91]. The Bi atom intensity depends on its depth within the column due to the channeling affect [32,33,37,92–97].

EELS resolution similarly improved, as did its sensitivity, allowing the spectroscopic identification of a single substitutional La atom in a Ca column in $CaTiO_3$ [98]. One spectacular result from the field of quasicrystals is shown in Fig. 8, which compares images of the decagonal $Al_{72}Ni_{20}Co_8$ phase taken simultaneously with the HAADF detector and a low angle ADF detector. The HAADF image shows the 2-nm clusters of transition metal columns very clearly, including the broken symmetry in the centers, which explains the origin of the quasiperiodic tiling

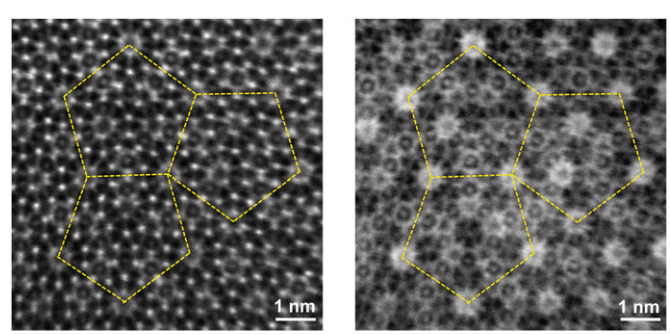

Fig. 8. ADF images of decagonal $Al_{72}Ni_{20}Co_8$, taken with a VG Microscopes HB501UX and Nion aberration corrector at 100 kV accelerating voltage. These images are simultaneously obtained with two different annular detectors, (left) HAADF detector, inner-angle ~50 mrad, (right) low angle ADF detector, inner-angle ~30 mrad. Occurrences of anomalous contrast seen in the low angle image indicate regions of high thermal vibration amplitude, and form a 2-nm-scale pentagonal quasiperiodic lattice (yellow). Adapted from Ref. [103]. (For interpretation of the references to color in this figure legend, the reader is referred to the web version of this article.)

[99–101]. However, with a lower detector angle the scattered intensity becomes sensitive to thermal vibration amplitude and particular sites, in a Penrose tiling pattern, show bright, indicating sites of enhanced thermal vibration amplitude [102].

Incorporating a similar aberration corrector into the VG Microscopes HB603U pushed its resolution into the sub-Angstrom regime, as shown in Fig. 9 through the resolution of the dumbbells in Si ⟨112⟩ at 0.78 Å [104,105]. Now images of the decagonal quasicrystal revealed every atomic site, including the light Al columns that were difficult to discern before correction. Fig. 10 compares images before and after aberration correction.

New applications appeared, notably in the field of Si_3N_4 ceramics, where it was possible for the first time to image the rare earth dopants necessary for improved mechanical properties [106–108]. At this time it was also realized that increasing the objective aperture size not only increased the transverse resolution, but also reduced the depth of field, making it less than the thickness of a typical transmission specimen. Now by changing focus one could obtain image slices from different depths, at least in amorphous or weakly channeling crystals. Images of single stray Hf atoms were obtained in this way in the nanometer thick gate dielectric of a semiconductor device, showing the three-dimensional location of each Hf atom and so revealing their density [109,110]. Such depth slicing is useful in catalysis [111,112], however, in crystals, the focusing of the probe at specific depths is opposed by the tendency of the column to channel the electrons. Depth sectioning can work only with relatively light columns [113,114]. Nevertheless, individual Au point defect configurations inside a Si nanowire were identified directly from a focal series [115]. Although small Au clusters were present on the nanowire surfaces, by focusing in the center of the nanowire the surface Au atoms became out of focus and invisible, so the internal point defect configurations could be observed. Single Y dopant atoms have also been imaged in a $\sum 13$ grain boundary of α-Al_2O_3, not edge on as usual, but their distribution within the grain boundary plane [116]. EELS is invaluable if the identity of the point defect is uncertain, and O interstitials in α-Si_3N_4 have been imaged and identified by EELS [117]. In $LiFePO_4$ Fe antisite defects have been imaged at the Li sites [118–120].

Phase contrast imaging in STEM is also dramatically different after aberration correction. With the flat phase region greatly expanded the collector aperture (reciprocally equivalent to the condenser aperture in TEM) can be enlarged up to an order of magnitude in the most recent instruments without severely damping the information transfer, and high resolution phase contrast images can be readily obtained with excellent signal to noise ratio [121]. An example of the use of phase contrast imaging to track octahedral rotations across a $BiFeO_3$/ $La_{0.7}Sr_{0.3}MnO_3$ interface is shown in Fig. 11, where it is seen that the octahedral rotations of the $BiFeO_3$ film are quenched for several unit cells near the interface [122].

These results were produced with 3rd order aberration correctors, but designs were already appearing for 5th order correctors [123–125] and results were not long in following. A resolution of 0.63 Å was achieved with [211] GaN [114,126,127] then 0.47 Å was obtained shortly after in ⟨114⟩ Ge [128,129], all with 300 kV accelerating voltage. STEM now firmly holds the record for image resolution, in accordance with the physics of incoherent imaging, and although noise remains limiting for the ultimate resolution, there is a broad scope for tradeoff between resolution and beam current. For spectroscopic applications one would normally sacrifice some spatial resolution for higher signal.

Another tradeoff concerns accelerating voltage. Particularly for the lighter elements with lower thresholds for knock on damage, there is a strong trend towards using lower accelerating voltage. Fig. 12 shows an image of a single monolayer of BN obtained in the spirit of the original Crewe images, collecting as many scattered electrons as possible with a medium angle ADF detector spanning 58–200 mr [130]. After Fourier filtering to remove noise and probe tails the image quality is very good, and B and N are easily distinguishable on the basis of their intensity alone, as in fact are impurity atoms. O is seen to substitute for N while C occurs in pairs, substituting for a BN unit. Also visible is a ring of six C atoms that previously was a small hole in the membrane but

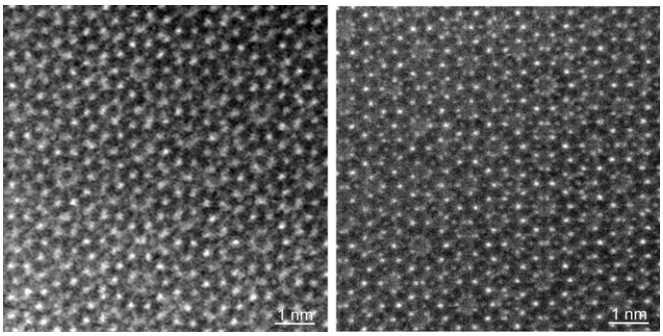

Fig. 10. Atomic-resolution Z-contrast images of the decagonal quasicrystal $Al_{72}Ni_{20}Co_8$ taken by a 300 kV VG Microscopes HB603U before (left) and after (right) installation of a Nion aberration corrector. Inner-angle of the detector was approximately 40 mrad for both images. Adapted from Ref. [103].

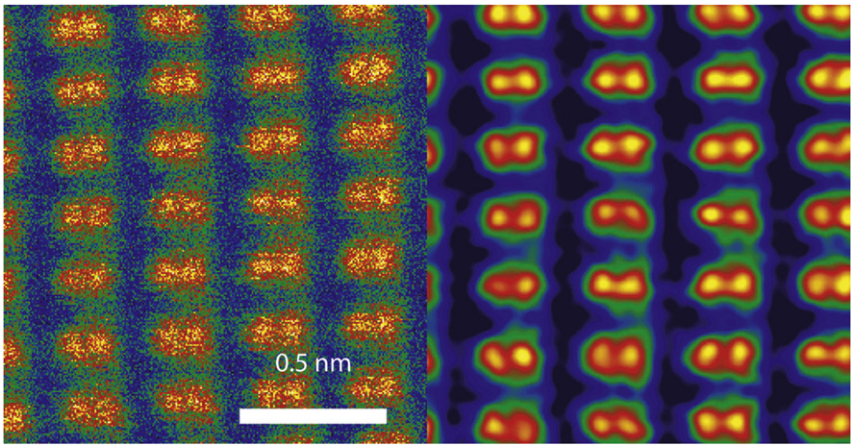

Fig. 9. Image of ⟨112⟩ Si recorded using a VG Microscopes HB603U with Nion aberration corrector operating at 300 kV (left). Image after low-pass filtering and unwarping (right). Every dumbbell shows a dip in the middle indicating resolution of the 0.78 Å spacing of the dumbbell. Reproduced from Ref. [104].

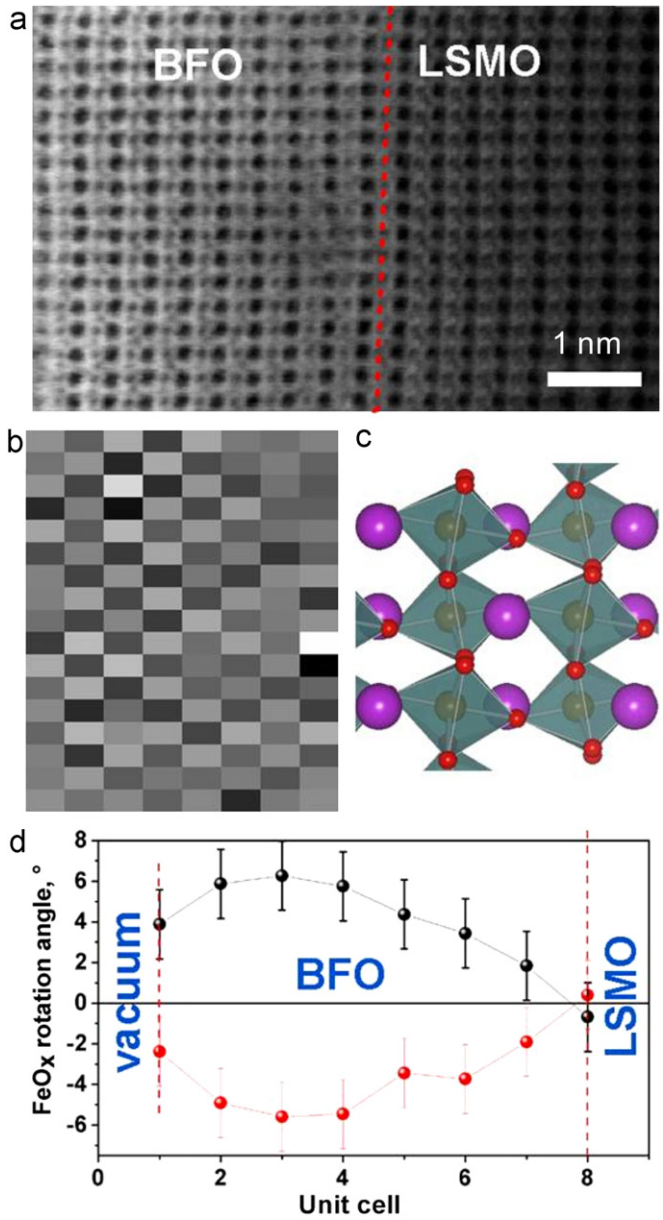

Fig. 11. Quantitative measurement of oxygen octahedral rotation angles using a VG Microscopes HB603U with Nion aberration corrector operating at 300 kV. (a) Bright field image of a $BiFeO_3$/ $La_{0.7}Sr_{0.3}MnO_3$ ultrathin film on $SrTiO_3$. (b) Corresponding two-dimensional map of in-plane octahedral rotation angles in BFO showing checkerboard ordering. (c) BFO structure in the rhombohedral (001) orientation showing the tilt pattern. (d) Line profile obtained from the map in (b), which was corrected for local Bi–Bi angle variations due to drift. Error bars in (d) are set equal to the standard deviation of the local Bi–Bi angles. Scale bar is 1 nm. Adapted from Ref. [122].

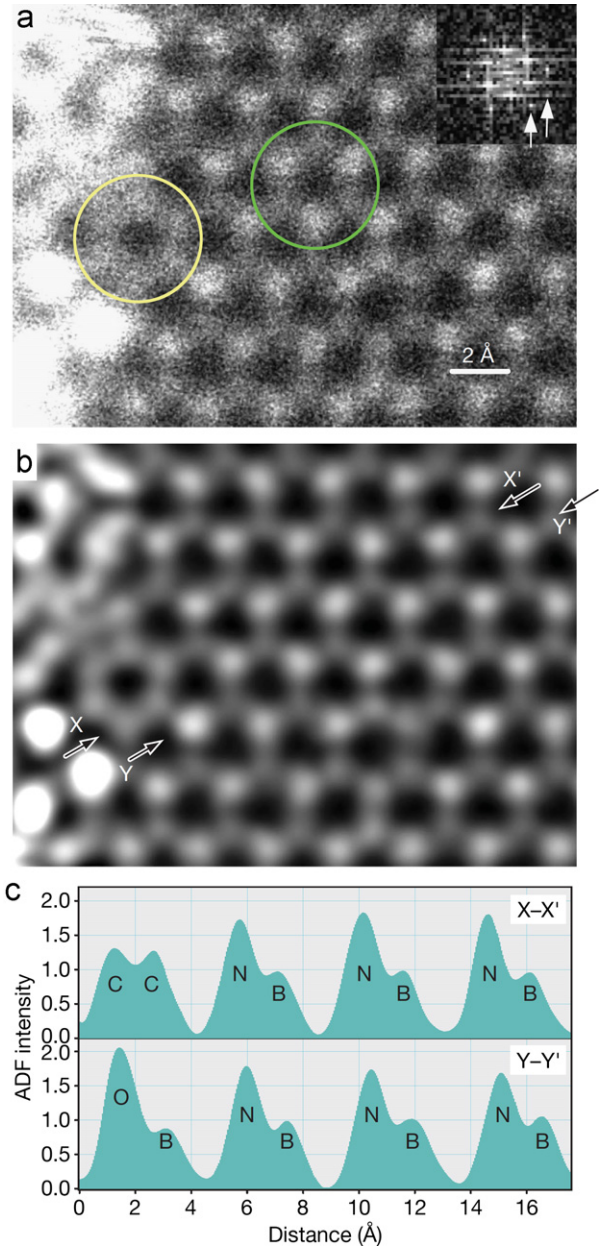

Fig. 12. Z-contrast STEM images of single-layer boron nitride. (a) As recorded, (b) rotated and corrected for distortion, and Fourier-filtered to reduce noise and probe tails. (c) Line profiles through the locations marked in (b), normalized to one for a single B atom. Inset at top right in (a) shows the Fourier transform of an image area away from the thicker regions. The two arrows point to $(11\bar{2}0)$ and $(20\bar{2}0)$ reflections of the hexagonal BN that correspond to recorded spacings of 1.26 and 1.09 Å. Taken with a Nion UltraSTEM operating at 60 kV. Reproduced from Ref. [130].

has been filled in with mobile C atoms. Now Z-contrast imaging is viable for light atoms as well as for heavy atoms [131].

Another detection mode useful for light elements is annular bright field, in which the annular detector covers approximately the outer half of the range of the probe-forming aperture. As proposed originally by Rose [132], it is a phase contrast mode of imaging and therefore has high sensitivity, but due to the high angular range it nevertheless shows incoherent characteristics [133–135]. The Z-contrast is much reduced compared to the ADF image which makes it easier to image light atom columns in the presence of heavy columns. A notable recent result is the imaging of H columns in hydrides [136,137].

The post-specimen optics on the latest columns are also much improved, allowing collection of almost 100% of the scattered electrons for most useful energy losses. Spectroscopic imaging is therefore much more efficient with sufficient signal to allow the two-dimensional mapping of core losses and spectral fine structure with atomic resolution [138–140]. Spectroscopic imaging of single atoms has even been demonstrated at the edges of graphene flakes where localized states were observed [141]. Spectroscopic imaging also visualized the disordered O sublattice in thin layers of Y_2O_3-stabilized ZrO_2 (YSZ) sandwiched between $SrTiO_3$ (STO) spacers [142], a system that provides a colossal enhancement of O ion conductivity near room temperature [143,144].

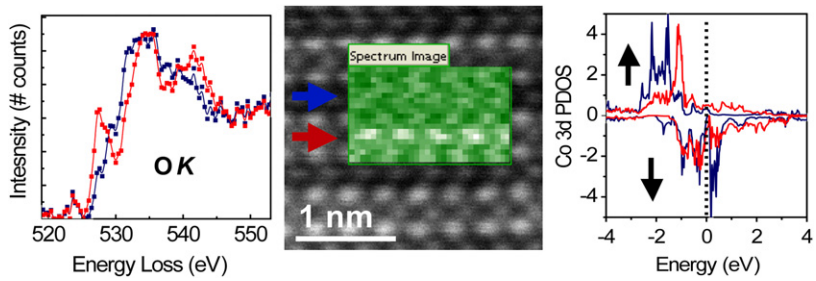

Fig. 13. Spin state mapping in $La_{0.5}Sr_{0.5}CoO_{3-\delta}$ thin films. The Z-contrast image shows the superlattice induced by vacancy ordering, the Co plane containing vacancies indicated by the blue arrow, the stoichiometric plane by the red arrow. The O K EELS edge (left) is different from the two planes, indicating a spin state superlattice. Density functional calculations (right) show the strong spin polarization in the blue planes near the Fermi level (dashed line). Reproduced from Ref. [145]. (For interpretation of the references to color in this figure legend, the reader is referred to the web version of this article.)

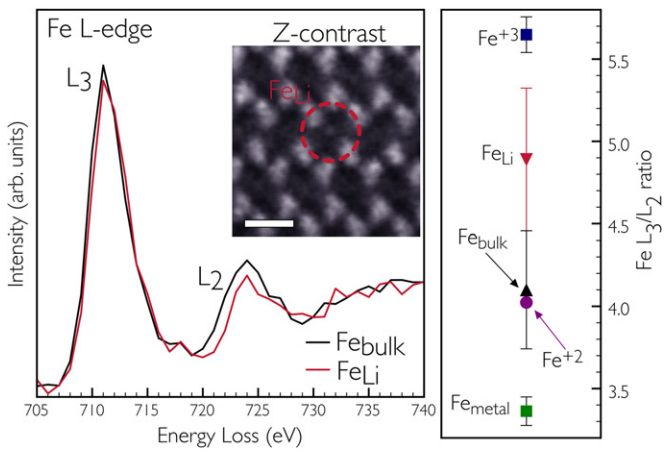

Fig. 14. Z-contrast image of $LiFePO_4$ showing a higher than expected intensity at some Li sites (red circle). EELS from such sites reveals the presence of Fe, and the Fe_{Li} $L_{2,3}$ ratio is higher than that of Fe in the bulk lattice sites Fe_{bulk}. Scale bar is 0.5 nm. Reproduced from Ref. [120]. (For interpretation of the references to color in this figure legend, the reader is referred to the web version of this article.)

Another recent example of fine structure mapping is the discovery of a spin state superlattice in strained nanopockets of $La_{0.5}Sr_{0.5}CoO_{3-\delta}$ thin films [145]. In cobaltites it is known that the EELS fine structure is sensitive to the Co spin state [146]. Fig. 13 shows how details of the fine structure enable the mapping of Co spin state in a small region of a $La_{0.5}Sr_{0.5}CoO_{3-\delta}$ thin film in which strong O vacancy ordering is present. Every other plane is oxygen deficient, a mechanism to accommodate the epitaxial strain with the substrate, leading to lattice expansion which is visible as a darker stripe in the Z-contrast image. The O K edge fine structure is quite different on these planes, whereas the Co $L_{2,3}$ ratio remains constant indicating no change in valence, ie., no charge ordering (as expected since these systems are metallic). The result indicates that Co in the O-deficient plane is in a high spin state while Co in the stoichiometric plane is in a low spin state. The result is confirmed by density functional calculations [145].

Another recent example of the interpretation of EELS fine structure is shown in Fig. 14 [120]. Antisite defects in the battery material $LiFePO_4$ cluster in particular channels, leaving others open to Li ion diffusion [119]. The result is important since maintaining open channels is necessary to allow charge and discharge of the battery. Measuring the Fe $L_{2,3}$ ratio of the antisite defects reveals an unexpected valence. Instead of the $+1$ expected if Fe simply substitutes for Li, the valence exceeds $+2$, higher than that of Fe in the bulk lattice sites. First-principles calculations reveal an attraction between an antisite Fe (Fe_{Li}) and a Li vacancy. This provides the mechanism for the clustering of Fe_{Li}. Although the attraction is not enough to keep the Li vacancies bound to the Fe_{Li}, by clustering the antisite defects in particular channels the Li vacancies are trapped. They shuttle back and forth between Fe_{Li} spending more time as neighbors and less time diffusing, resulting in a net energy reduction. This unusual energy-lowering mechanism is a feature of the one-dimensional nature of the Li diffusion paths, and suggests exploring temperatures for growth and/or annealing that optimize segregation and maximize Li diffusion.

5. Future Trends

The advantage of a reduced accelerating voltage for avoiding knock-on damage in materials such as graphene has already been pointed out. Although atomic resolution can be achieved at much lower voltages with the 5th-order correctors, chromatic aberration effects become increasingly severe. Chromatic aberration causes intensity to be removed from the peak of the probe into the tail [147], thus reducing the resolution and contrast of the image. This issue is stimulating the development of chromatic aberration correctors and monochromators [148–151]. EELS of course benefits dramatically from the development of a monochromator, particularly for applications such as band gap mapping [152,153] and the availability of an atomic-resolution monochromated probe would be extremely valuable. Recent improvements to X-ray detectors have improved their efficiency while avoiding the need for liquid nitrogen cooling, so they may now be incorporated into aberration corrected columns without the fear of introducing instabilities. Atomic-resolution mapping using X-ray fluorescence spectroscopy has been recently achieved [154,155], and can show improved spatial resolution compared to EELS, albeit if more noisy, as X-ray signals are typically more localized [156].

Another emerging trend is the incorporation of in situ stages into aberration-corrected microscopes for heating or maintaining a gas ambient [157,158]. Such stages would be particularly valuable in the field of catalysis [159–163]. Cooling stages remain a challenge because of the need for refridgerant and the associated inherent instabilities. Another emerging trend is likely to be the mapping of functionality in the aberration-corrected STEM [164]. The possibility of detecting signals such as cathodoluminescence or electron beam induced current offers the possibility to directly correlate local functionality with the local atomic and electronic structure seen in the normal imaging and EELS signals. The low signals anticipated for the secondary excitations can be compensated for by increasing the beam current. Aberration correction not only allows smaller probes, it can deliver much larger currents into nanoscale probes than an uncorrected microscope. Switching from high current to low current mode may allow the first direct correlation of local electronic and optical properties with atomic structure and impurity sites.

Albert Crewe would surely be gratified by the recent progress, the associated major growth in applications, and the potential that still awaits for the instrument that he pioneered a half century ago.

Acknowledgments

The author is grateful to E. Abe, N.D. Browning, A.Y. Borisevich, M.F. Chisholm, N. Dellby, J. Gazguez, J.C. Idrobo, D.E. Jesson, O.L. Krivanek, J.W. Lee, C. Leighton, J.T. Luck, W.D. Luo, A.R. Lupini, A.J. McGibbon, M.F. Murfitt, J. Narayan, V. Nicolosi, P.D. Nellist, C.S. Own, M.P. Oxley, S.T. Pantelides, T.J. Pennycook, Y. Peng, M. Prange, W.H. Sides, M. Sharma, Z.S. Szilagyi, M.A. Torija and M. Varela for permission to reproduce materials and for research collaborations. This work was supported by the US Department of Energy, Office of Basic Energy Sciences, Materials Sciences and Engineering Division.

References

[1] S.J. Pennycook, P.D. Nellist, Scanning Transmission Electron Microscopy: Imaging and Analysis, Springer, New York, Dordrecht, Heidelberg, London, 2011.
[2] M. Knoll, E. Ruska, Das Elektronenmikroskop, Zeitschrift für Physik A 78 (1932) 318–339.
[3] M. von Ardenne, Das Elektronen-rastermikroskop. theoretische grundlagen, Zeitschrift für Physik 109 (1938) 553–572.
[4] M. von Ardenne, Das Elektronen-rastermikroskop. Praktische Ausführung, Zeitschrift für Technische Physik 19 (1938) 407–416.
[5] M. von Ardenne, On the history of scanning electron microscopy, of the electron microprobe, and of early contributions to transmission electron microscopy, in: P.W. Hawkes (Ed.), Advances in Imaging and Electron Physics, the Beginnings of Electron-Microscopy, Academic Press, Orlando, FL, 1985, pp. 1–21.
[6] M. von Ardenne, Reminiscences on the origins of the scanning electron microscope and the electron microprobe, in: T. Mulvey (Ed.), Advances in Imaging and Electron Physics, the Growth of Electron Microscopy, Acadenic Press, San Diego, 1996, pp. 635–652.
[7] A.V. Crewe, Scanning electron microscopes—is high resolution possible? Science 154 (1966) 729–738.
[8] A.V. Crewe, J. Wall, L.M. Welter, A high-resolution scanning transmission electron microscope, Journal of Applied Physics 39 (1968) 5861–5868.
[9] A.V. Crewe, J. Wall, A scanning microscope with 5 Å resolution, Journal of Molecular Biology 48 (1970) 375–393.
[10] A.V. Crewe, J. Wall, J. Langmore, Visibility of single atoms, Science 168 (1970) 1338–1340.
[11] A.V. Crewe, The work of Albert Victor Crewe on the scanning transmission electron microscope and related topics, in: P.W. Hawkes (Ed.), Advances in Imaging and Electron Physics, Elsevier, Amsterdam, 2009, pp. 1–61.
[12] A.V. Crewe, High resolution scanning microscopy of biological specimens, Philosophical Transactions of the Royal Society B 261 (1971) 61–70.
[13] J. Wall, J. Langmore, M. Isaacson, A.V. Crewe, Scanning-transmission electron-microscopy at high-resolution, Proceedings of the National Academy of Sciences of the United States of America 71 (1974) 1–5.
[14] J.M. Cowley, Image contrast in a transmission scanning electron microscope, Applied Physics Letters 15 (1969) 58–59.
[15] E. Zeitler, M.G.R. Thomson, Scanning transmission electron microscopy, Optik 31 (1970) 258–280 and 359–366.
[16] M. Isaacson, D. Johnson, Microanalysis of light-elements using transmitted energy-loss electrons, Ultramicroscopy 1 (1975) 33–52.
[17] I.R.M. Wardell, P.E. Bovey, A history of Vacuum Generators' 100 kV scanning transmission electron microscope, in: P.W. Hawkes (Ed.), Advances in Imaging and Electron Physics, Elsevier, 2009, pp. 221–285.
[18] L.M. Brown, Scanning transmission electron microscopy: microanalysis for the microelectronic age, Journal of Physics F 11 (1981) 1–26.
[19] A.M. Donald, A.J. Craven, Study of grain-boundary segregation in Cu–Bi alloys using STEM, Philosophical Magazine A 39 (1979) 1–11.
[20] M.M.J. Treacy, A. Howie, C.J. Wilson, Z-contrast of platinum and palladium catalysts, Philosophical Magazine A 38 (1978) 569–585.
[21] A. Howie, Image-contrast and localized signal selection techniques, Journal of Microscopy (Oxford) 117 (1979) 11–23.
[22] M.M.J. Treacy, A. Howie, S.J. Pennycook, Z-contrast of supported catalyst particles on the STEM, in: T. Mulvey (Ed.), Electron Microscopy and Analysis 1979, Institute of Physics, Brighton, 1980, pp. 261–266.
[23] S.J. Pennycook, J. Narayan, Direct imaging of dopant distributions in silicon by scanning-transmission electron-microscopy, Applied Physics Letters 45 (1984) 385–387.
[24] Rayleigh, Lord, On the theory of optical images with special reference to the microscope, Philosophical Magazine 42 (5) (1896) 167–195.
[25] J.M. Cowley, Scanning transmission electron microscopy and microdiffraction techniques, Bulletin of Materials Science 6 (1984) 477–490.
[26] A. Engel, J.W. Wiggins, D.C. Woodruff, Comparison of calculated images generated by 6 modes of transmission electron-microscopy, Journal of Applied Physics 45 (1974) 2739–2747.
[27] D.L. Misell, G.W. Stroke, M. Halioua, Coherent and incoherent imaging in scanning-transmission electron-microscope, Journal of Physics D 7 (1974) L113–L117.
[28] G. Ade, On the incoherent imaging in the scanning transmission electron microscope (STEM), Optik 49 (1977) 113–116.
[29] J.M. Cowley, Scanning-transmission electron-microscopy of thin specimens, Ultramicroscopy 2 (1976) 3–16.
[30] S.J. Pennycook, L.A. Boatner, Chemically sensitive structure-imaging with a scanning-transmission electron-microscope, Nature 336 (1988) 565–567.
[31] S.J. Pennycook, Z-contrast STEM for materials science, Ultramicroscopy 30 (1989) 58–69.
[32] S.J. Pennycook, D.E. Jesson, High-resolution incoherent imaging of crystals, Physical Review Letters 64 (1990) 938–941.
[33] S.J. Pennycook, D.E. Jesson, High-resolution Z-contrast imaging of crystals, Ultramicroscopy 37 (1991) 14–38.
[34] K. Kambe, Visualization of Bloch waves of high-energy electrons in high-resolution electron-microscopy, Ultramicroscopy 10 (1982) 223–227.
[35] D.E. Jesson, S.J. Pennycook, Incoherent imaging of thin specimens using coherently scattered electrons, Proceedings of the Royal Society of London A 441 (1993) 261–281.
[36] D.E. Jesson, S.J. Pennycook, Incoherent imaging of crystals using thermally scattered electrons, Proceedings of the Royal Society of London A 449 (1995) 273–293.
[37] R.F. Loane, P. Xu, J. Silcox, Incoherent imaging of zone axis crystals with ADF STEM, Ultramicroscopy 40 (1992) 121–138.
[38] D.E. Jesson, S.J. Pennycook, J.M. Baribeau, D.C. Houghton, Direct imaging of surface cusp evolution during strained-layer epitaxy and implications for strain relaxation, Physical Review Letters 71 (1993) 1744–1747.
[39] D.E. Jesson, S.J. Pennycook, J.Z. Tischler, J.D. Budai, J.M. Baribeau, D.C. Houghton, Interplay between evolving surface-morphology, atomic-scale growth modes, and ordering during Si_xGe_{1-x} epitaxy, Physical Review Letters 70 (1993) 2293–2296.
[40] M.F. Chisholm, S.J. Pennycook, Structural origin of reduced critical currents at $YBa_2Cu_3O_{7-\delta}$ grain-boundaries, Nature 351 (1991) 47–49.
[41] H.S. von Harrach, Medium-voltage field-emission STEM—the ultimate AEM, Microscopy Microanalysis Microstructures 5 (1994) 153–164.
[42] H.S. von Harrach, A.W. Nicholls, D.E. Jesson, S.J. Pennycook, First results of a 300 kV high-resolution field-emission STEM, in: A.J. Craven (Ed.), Institute of Physics Conference Series No. 138, Institute of Physics, Bristol, 1993, pp. 499–502.
[43] H.S. von Harrach, Development of the 300 kV vacuum generator STEM (1985–1996), in: P.W. Hawkes (Ed.), Advances in Imaging and Electron Physics, Elsevier, 2009, pp. 287–323.
[44] S.J. Pennycook, N.D. Browning, M.M. McGibbon, A.J. McGibbon, D.E. Jesson, M.F. Chisholm, Direct determination of interface structure and bonding with the scanning transmission electron microscope, Philosophical Transactions of the Royal Society of London A 354 (1996) 2619–2634.
[45] A.J. McGibbon, S.J. Pennycook, J.E. Angelo, Direct observation of dislocation core structures in CdTe/GaAs(001), Science 269 (1995) 519–521.
[46] Y. Xin, S.J. Pennycook, N.D. Browning, P.D. Nellist, S. Sivananthan, F. Omnes, B. Beaumont, J.P. Faurie, P. Gibart, Direct observation of the core structures of threading dislocations in GaN, Applied Physics Letters 72 (1998) 2680–2682.
[47] P.D. Nellist, S.J. Pennycook, Direct imaging of the atomic configuration of ultradispersed catalysts, Science 274 (1996) 413–415.
[48] N.D. Browning, S.J. Pennycook, M.F. Chisholm, M.M. McGibbon, A.J. McGibbon, Observation of structural units at symmetric [001] tilt boundaries in $SrTiO_3$, Interface Science 2 (1995) 397–423.
[49] M.M. McGibbon, N.D. Browning, A.J. McGibbon, S.J. Pennycook, The atomic structure of asymmetric [001] tilt boundaries in $SrTiO_3$, Philosophical Magazine A 73 (1996) 625–641.
[50] E.C. Dickey, V.P. Dravid, P.D. Nellist, D.J. Wallis, S.J. Pennycook, Three-dimensional atomic structure of NiO–ZrO_2(cubic) interfaces, Acta Materialia 46 (1998) 1801–1816.
[51] D.A. Muller, S. Subramanian, P.E. Batson, J. Silcox, S.L. Sass, Structure, chemistry and bonding at grain boundaries in Ni_3Al.1. The role of boron in ductilizing grain boundaries, Acta Materialia 44 (1996) 1637–1645.
[52] M.F. Chisholm, A. Maiti, S.J. Pennycook, S.T. Pantelides, Atomic configurations and energetics of arsenic impurities in a silicon grain boundary, Physical Review Letters 81 (1998) 132–135.
[53] Y. Yan, M.F. Chisholm, G. Duscher, A. Maiti, S.J. Pennycook, S.T. Pantelides, Impurity-induced structural transformation of a MgO grain boundary, Physical Review Letters 81 (1998) 3675–3678.
[54] A.V. Crewe, M. Isaacson, D. Johnson, Electron energy loss spectra of nucleic acid bases, Nature 231 (1971) 262–263.
[55] D. McMullan, J.M. Rodenburg, Y. Murooka, A.J. McGibbon, Parallel EELS CCD detector for a VG HB501 STEM, Institute of Physics Conference Series No. 98 (1990) 55–58.

[56] S.J. Pennycook, M. Varela, A.R. Lupini, M.P. Oxley, M.F. Chisholm, Atomic-resolution spectroscopic imaging: past, present and future, Journal of Electron Microscopy 58 (2009) 87–97.
[57] N.D. Browning, M.F. Chisholm, S.J. Pennycook, Atomic-resolution chemical-analysis using a scanning-transmission electron-microscope, Nature 366 (1993) 143–146.
[58] N.D. Browning, M.F. Chisholm, S.J. Pennycook, Atomic-resolution electron energy loss spectroscopy in the scanning transmission electron microscope, in: 27th Annual Proceedings of Microbeam Analysis Society, VCH, Los Angeles, 1993, pp. S270–271.
[59] N.D. Browning, M.F. Chisholm, S.J. Pennycook, Atomic-resolution chemical analysis using a scanning transmission electron microscope (vol 366, pg 143, 1993), Nature 444 (2006) 235–235.
[60] P.E. Batson, Simultaneous STEM imaging and electron energy-loss spectroscopy with atomic-column sensitivity, Nature 366 (1993) 727–728.
[61] D.A. Muller, Y. Tzou, R. Raj, J. Silcox, Mapping sp(2) and sp(3) states of carbon at subnanometer spatial-resolution, Nature 366 (1993) 725–727.
[62] G. Duscher, N.D. Browning, S.J. Pennycook, Atomic column resolved electron energy-loss spectroscopy, Physica Status Solidi A 166 (1998) 327–342.
[63] P.E. Batson, Atomic and electronic structure of a dissociated 60 degrees misfit dislocation in $Ge_xSi_{(1-x)}$, Physical Review Letters 83 (1999) 4409–4412.
[64] N.D. Browning, H.O. Moltaji, J.P. Buban, Investigation of three-dimensional grain-boundary structures in oxides through multiple-scattering analysis of spatially resolved electron-energy-loss spectra, Physical Review B 58 (1998) 8289–8300.
[65] D.A. Muller, T. Sorsch, S. Moccio, F.H. Baumann, K. Evans-Lutterodt, G. Timp, The electronic structure at the atomic scale of ultrathin gate oxides, Nature 399 (1999) 758–761.
[66] X. Fan, E.C. Dickey, P.C. Eklund, K.A. Williams, L. Grigorian, R. Buczko, S.T. Pantelides, S.J. Pennycook, Atomic arrangement of iodine atoms inside single-walled carbon nanotubes, Physical Review Letters 84 (2000) 4621–4624.
[67] R.F. Klie, N.D. Browning, Atomic scale characterization of oxygen vacancy segregation at $SrTiO_3$ grain boundaries, Applied Physics Letters 77 (2000) 3737–3739.
[68] S. Stemmer, A. Sane, N.D. Browning, T.J. Mazanec, Characterization of oxygen-deficient $SrCoO_{3-\delta}$ by electron energy-loss spectroscopy and Z-contrast imaging, Solid State Ionics 130 (2000) 71–80.
[69] C. Jeanguillaume, C. Colliex, Spectrum-image: the next step in EELS digital acquisition and processing, Ultramicroscopy 28 (1989) 252–257.
[70] J.A. Hunt, D.B. Williams, Electron energy-loss spectrum-imaging, Ultramicroscopy 38 (1991) 47–73.
[71] R.D. Leapman, L.A. Grunes, Anomalous L_3–L_2 white-line ratios in the 3d transition-metals, Physical Review Letters 45 (1980) 397–401.
[72] R.D. Leapman, L.A. Grunes, P.L. Fejes, Study of the L_{23} edges in the 3d transition-metals and their oxides by electron-energy-loss spectroscopy with comparisons to theory, Physical Review B 26 (1982) 614–635.
[73] H. Kurata, C. Colliex, Electron-energy-loss core-edge structures in manganese oxides, Physical Review B 48 (1993) 2102–2108.
[74] L.A. Grunes, R.D. Leapman, C.N. Wilker, R. Hoffmann, A.B. Kunz, Oxygen-K near-edge fine-structure—an electron-energy-loss investigation with comparisons to new theory for selected 3d transition-metal oxides, Physical Review B 25 (1982) 7157–7173.
[75] A. Ohtomo, H.Y. Hwang, A high-mobility electron gas at the $LaAlO_3/SrTiO_3$ heterointerface, Nature 427 (2004) 423–426.
[76] A. Ohtomo, D.A. Muller, J.L. Grazul, H.Y. Hwang, Artificial charge-modulation in atomic-scale perovskite titanate superlattices, Nature 419 (2002) 378–380.
[77] J. Verbeeck, O.I. Lebedev, G. Van Tendeloo, J. Silcox, B. Mercey, M. Hervieu, A.M. Haghiri-Gosnet, Electron energy-loss spectroscopy study of a $(LaMnO_3)_8(SrMnO_3)_4$ heterostructure, Applied Physics Letters 79 (2001) 2037–2039.
[78] M. Varela, A.R. Lupini, S.J. Pennycook, Z. Sefrioui, J. Santamaria, Nanoscale analysis of $YBa_2Cu_3O_{7-x}/La_{0.67}Ca_{0.33}MnO_3$ interfaces, Solid-State Electronics 47 (2003) 2245–2248.
[79] S.D. Berger, S.J. Pennycook, Detection of nitrogen at (100) platelets in diamond, Nature 298 (1982) 635–637.
[80] O. Scherzer, Sphärische und chromatische Korrektur von Elektronen-Linsen, Optik 2 (1947) 114–132.
[81] H. Rose, History of direct aberration correction, in: P.W. Hawkes (Ed.), Advances in Imaging and Electron Physics, Elsevier, Amsterdam, The Netherlands, 2008, pp. 3–39.
[82] P.W. Hawkes, Aberration correction past and present, Philosophical Transactions of the Royal Society A 367 (2009) 3637–3664.
[83] O.L. Krivanek, N. Dellby, M.F. Murfitt, Aberration correction in electron microscopy, in: J. Orloff (Ed.), Handbook of Charged Particle Optics, CRC Press, Boca Raton, 2009, pp. 601–640.
[84] A.V. Crewe, High-resolution scanning-transmission electron-microscopy, Science 221 (1983) 325–330.
[85] A.V. Crewe, Some chicago aberrations, Microscopy and Microanalysis 10 (2004) 414–419.
[86] A.V. Crewe, D.B. Salzman, On the optimum resolution for a corrected STEM, Ultramicroscopy 9 (1982) 373–377.
[87] J.Y. Ximen, A.V. Crewe, Correction of spherical and coma aberrations with a sextupole round lens sextupole system, Optik 69 (1985) 141–146.
[88] M. Haider, S. Uhlemann, E. Schwan, H. Rose, B. Kabius, K. Urban, Electron microscopy image enhanced, Nature 392 (1998) 768–769.
[89] O.L. Krivanek, N. Dellby, A.R. Lupini, Towards sub-angstrom electron beams, Ultramicroscopy 78 (1999) 1–11.
[90] N. Dellby, O.L. Krivanek, P.D. Nellist, P.E. Batson, A.R. Lupini, Progress in aberration-corrected scanning transmission electron microscopy, Journal of Electron Microscopy 50 (2001) 177–185.
[91] A.R. Lupini, S.J. Pennycook, Localization in elastic and inelastic scattering, Ultramicroscopy 96 (2003) 313–322.
[92] J. Fertig, H. Rose, Resolution and contrast of crystalline objects in high-resolution scanning-transmission electron-microscopy, Optik 59 (1981) 407–429.
[93] R.F. Loane, E.J. Kirkland, J. Silcox, Visibility of single heavy-atoms on thin crystalline silicon in simulated annular dark-field STEM images, Acta Crystallographica A 44 (1988) 912–927.
[94] S.J. Pennycook, D.E. Jesson, Atomic resolution Z-contrast imaging of interfaces, Acta Metallurgica et Materialia 40 (1992) S149–S159.
[95] S. Hillyard, R.F. Loane, J. Silcox, Annular dark-field imaging—resolution and thickness effects, Ultramicroscopy 49 (1993) 14–25.
[96] S. Hillyard, J. Silcox, Thickness effects in ADF STEM zone-axis images, Ultramicroscopy 52 (1993) 325–334.
[97] K. Nakamura, H. KaKibayashi, K. Kanehori, N. Tanaka, Position dependence of the visibility of a single gold atom in silicon crystals in HAADF-STEM image simulation, Journal of Electron Microscopy 46 (1997) 33–43.
[98] M. Varela, S.D. Findlay, A.R. Lupini, H.M. Christen, A.Y. Borisevich, N. Dellby, O.L. Krivanek, P.D. Nellist, M.P. Oxley, L.J. Allen, S.J. Pennycook, Spectroscopic imaging of single atoms within a bulk solid, Physical Review Letters 92 (2004) 095502.
[99] Y.F. Yan, S.J. Pennycook, Alloys—atomic structure of the quasicrystal Al72Ni20Co8, Nature 403 (2000) 266–267.
[100] Y.F. Yan, S.J. Pennycook, Chemical ordering in $Al_{72}Ni_{20}Co_8$ decagonal quasicrystals, Physical Review Letters 86 (2001) 1542–1545.
[101] P.J. Steinhardt, H.C. Jeong, K. Saitoh, M. Tanaka, E. Abe, A.P. Tsai, Experimental verification of the quasi-unit-cell model of quasicrystal structure, Nature 396 (1998) 55–57.
[102] E. Abe, S.J. Pennycook, A.P. Tsai, Direct observation of a local thermal vibration anomaly in a quasicrystal, Nature 421 (2003) 347–350.
[103] E. Abe, Structure of quasicrystals, in: S.J. Pennycook, P.D. Nellist (Eds.), Scanning Transmission Electron Microscopy: Imaging and Analysis, Springer, New York, 2011, pp. 583–614.
[104] P.D. Nellist, M.F. Chisholm, N. Dellby, O.L. Krivanek, M.F. Murfitt, Z.S. Szilagyi, A.R. Lupini, A. Borisevich, W.H. Sides, S.J. Pennycook, Direct sub-angstrom imaging of a crystal lattice, Science 305 (2004) 1741-1741.
[105] Y. Peng, M.P. Oxley, A.R. Lupini, M.F. Chisholm, S.J. Pennycook, Spatial resolution and information transfer in scanning transmission electron microscopy, Microscopy and Microanalysis 14 (2008) 36–47.
[106] G.B. Winkelman, C. Dwyer, T.S. Hudson, D. Nguyen-Manh, M. Doblinger, R.L. Satet, M.J. Hoffmann, D.J.H. Cockayne, Three-dimensional organization of rare-earth atoms at grain boundaries in silicon nitride, Applied Physics Letters 87 (2005) 061911.
[107] A. Ziegler, J.C. Idrobo, M.K. Cinibulk, C. Kisielowski, N.D. Browning, R.O. Ritchie, Interface structure and atomic bonding characteristics in silicon nitride ceramics, Science 306 (2004) 1768–1770.
[108] N. Shibata, S.J. Pennycook, T.R. Gosnell, G.S. Painter, W.A. Shelton, P.F. Becher, Observation of rare-earth segregation in silicon nitride ceramics at subnanometre dimensions, Nature 428 (2004) 730–733.
[109] K. van Benthem, A.R. Lupini, M. Kim, H.S. Baik, S. Doh, J.H. Lee, M.P. Oxley, S.D. Findlay, L.J. Allen, J.T. Luck, S.J. Pennycook, Three-dimensional imaging of individual hafnium atoms inside a semiconductor device, Applied Physics Letters 87 (2005) 034104.
[110] K. van Benthem, A.R. Lupini, M.P. Oxley, S.D. Findlay, L.J. Allen, S.J. Pennycook, A.D.F. Three-dimensional, imaging of individual atoms by through-focal series scanning transmission electron microscopy, Ultramicroscopy 106 (2006) 1062–1068.
[111] S.W. Wang, A.Y. Borisevich, S.N. Rashkeev, M.V. Glazoff, K. Sohlberg, S.J. Pennycook, S.T. Pantelides, Dopants adsorbed as single atoms prevent degradation of catalysts, Nature Materials 3 (2004) 143–146.
[112] A.Y. Borisevich, A.R. Lupini, S.J. Pennycook, Depth sectioning with the aberration-corrected scanning transmission electron microscope, Proceedings of the National Academy of Sciences of the United States of America 103 (2006) 3044–3048.
[113] A.Y. Borisevich, A.R. Lupini, S. Travaglini, S.J. Pennycook, Depth sectioning of aligned crystals with the aberration-corrected scanning transmission electron microscope, Journal of Electron Microscopy 55 (2006) 7–12.
[114] A.R. Lupini, A.Y. Borisevich, J.C. Idrobo, H.M. Christen, M. Biegalski, S.J. Pennycook, Characterizing the two- and three-dimensional resolutions of an improved aberration-corrected STEM, Microscopy and Microanalysis 15 (2009) 441–453.
[115] S.H. Oh, K. van Benthem, S.I. Molina, A.Y. Borisevich, W.D. Luo, P. Werner, N.D. Zakharov, D. Kumar, S.T. Pantelides, S.J. Pennycook, Point defect configurations of supersaturated Au atoms inside Si nanowires, Nano Letters 8 (2008) 1016–1019.
[116] N. Shibata, S.D. Findlay, S. Azuma, T. Mizoguchi, T. Yamamoto, Y. Ikuhara, Atomic-scale imaging of individual dopant atoms in a buried interface, Nature Materials 8 (2009) 654–658.

[117] J.C. Idrobo, M.P. Oxley, W. Walkosz, R.F. Klie, S. Ogut, B. Mikijelj, S.J. Pennycook, S.T. Pantelides, Identification and lattice location of oxygen impurities in alpha-Si_3N_4, Applied Physics Letters 95 (2009) 164101.
[118] S.Y. Chung, S.Y. Choi, T. Yamamoto, Y. Ikuhara, Atomic-scale visualization of antisite defects in $LiFePO_4$, Physical Review Letters 100 (2008) 125502.
[119] S.Y. Chung, S.Y. Choi, T. Yamamoto, Y. Ikuhara, Orientation-dependent arrangement of antisite defects in lithium iron(II) phosphate crystals, Angewandte Chemie—International Edition 48 (2009) 543–546.
[120] J. Lee, W. Zhou, J.C. Idrobo, S.J. Pennycook, S.T. Pantelides, Vacancy-driven anisotropic defect distribution in the battery-cathode material $LiFePO_4$, Physical Review Letters 107 (2011) 085507.
[121] S.J. Pennycook, M.F. Chisholm, A.R. Lupini, M. Varela, A.Y. Borisevich, M.P. Oxley, W.D. Luo, K. van Benthem, S.H. Oh, D.L. Sales, S.I. Molina, J. Garcia-Barriocanal, C. Leon, J. Santamaria, S.N. Rashkeev, S.T. Pantelides, Aberration-corrected scanning transmission electron microscopy: from atomic imaging and analysis to solving energy problems, Philosophical Transactions of the Royal Society of London A 367 (2009) 3709–3733.
[122] A.Y. Borisevich, H.J. Chang, M. Huijben, M.P. Oxley, S. Okamoto, M.K. Niranjan, J.D. Burton, E.Y. Tsymbal, Y.H. Chu, P. Yu, R. Ramesh, S.V. Kalinin, S.J. Pennycook, Suppression of octahedral tilts and associated changes in electronic properties at epitaxial oxide heterostructure interfaces, Physical Review Letters 105 (2010) 087204.
[123] M. Haider, S. Uhlemann, J. Zach, Upper limits for the residual aberrations of a high-resolution aberration-corrected STEM, Ultramicroscopy 81 (2000) 163–175.
[124] O.L. Krivanek, P.D. Nellist, N. Dellby, M.F. Murfitt, Z. Szilagyi, Towards sub-0.5 angstrom electron beams, Ultramicroscopy 96 (2003) 229–237.
[125] H. Müller, S. Uhlemann, P. Hartel, M. Haider, Advancing the hexapole Cs-corrector for the scanning transmission electron microscope, Microscopy and Microanalysis 12 (2006) 442–455.
[126] H. Sawada, F. Hosokawai, T. Kaneyama, T. Ishizawa, M. Terao, M. Kawazoe, T. Sannomiya, T. Tomita, Y. Kondo, T. Tanaka, Y. Oshima, Y. Tanishiro, N. Yamamoto, K. Takayanagi, Achieving 63 pm resolution in scanning transmission electron microscope with spherical aberration corrector, Japanese Journal of Applied Physics 46 (2007) L568–L570.
[127] C. Kisielowski, B. Freitag, M. Bischoff, H. van Lin, S. Lazar, G. Knippels, P. Tiemeijer, M. van der Stam, S. von Harrach, M. Stekelenburg, M. Haider, S. Uhlemann, H. Muller, P. Hartel, B. Kabius, D. Miller, I. Petrov, E.A. Olson, T. Donchev, E.A. Kenik, A.R. Lupini, J. Bentley, S.J. Pennycook, I.M. Anderson, A.M. Minor, A.K. Schmid, T. Duden, V. Radmilovic, Q.M. Ramasse, M. Watanabe, R. Erni, E.A. Stach, P. Denes, U. Dahmen, Detection of single atoms and buried defects in three dimensions by aberration-corrected electron microscope with 0.5 - Ångstrom information limit, Microscopy and Microanalysis 14 (2008) 469–477.
[128] R. Erni, M.D. Rossell, C. Kisielowski, U. Dahmen, Atomic-resolution imaging with a sub-50 pm electron probe, Physical Review Letters 102 (2009) 096101.
[129] H. Sawada, Y. Tanishiro, N. Ohashi, T. Tomita, F. Hosokawa, T. Kaneyama, Y. Kondo, K. Takayanagi, STEM imaging of 47 pm-separated atomic columns by a spherical aberration-corrected electron microscope with a 300 kV cold field emission gun, Journal of Electron Microscopy 58 (2009) 357–361.
[130] O.L. Krivanek, M.F. Chisholm, V. Nicolosi, T.J. Pennycook, G.J. Corbin, N. Dellby, M.F. Murfitt, C.S. Own, Z.S. Szilagyi, M.P. Oxley, S.T. Pantelides, S.J. Pennycook, Atom-by-atom structural and chemical analysis by annular dark-field electron microscopy, Nature 464 (2010) 571–574.
[131] O.L. Krivanek, N. Dellby, M.F. Murfitt, M.F. Chisholm, T.J. Pennycook, K. Suenaga, V. Nicolosi, Gentle STEM: ADF imaging and EELS at low primary energies, Ultramicroscopy 110 (2010) 935–945.
[132] H. Rose, Phase-contrast in scanning-transmission electron-microscopy, Optik 39 (1974) 416–436.
[133] E. Okunishi, I. Ishikawa, H. Sawada, F. Hosokawa, M. Hori, Y. Kondo, Visualization of light elements at ultrahigh resolution by STEM annular bright field microscopy, Microscopy and Microanalysis 15 (2009) 164–165.
[134] S.D. Findlay, N. Shibata, H. Sawada, E. Okunishi, Y. Kondo, T. Yamamoto, Y. Ikuhara, Robust atomic resolution imaging of light elements using scanning transmission electron microscopy, Applied Physics Letters 95 (2009) 191913.
[135] S.D. Findlay, N. Shibata, H. Sawada, E. Okunishi, Y. Kondo, Y. Ikuhara, Dynamics of annular bright field imaging in scanning transmission electron microscopy, Ultramicroscopy 110 (2010) 903–923.
[136] S.D. Findlay, T. Saito, N. Shibata, Y. Sato, J. Matsuda, K. Asano, E. Akiba, T. Hirayama, Y. Ikuhara, Direct imaging of hydrogen within a crystalline environment, Applied Physics Express 3 (2010) 116603.
[137] R. Ishikawa, E. Okunishi, H. Sawada, Y. Kondo, F. Hosokawa, E. Abe, Direct imaging of hydrogen-atom columns in a crystal by annular bright-field electron microscopy, Nature Materials 10 (2011) 278–281.
[138] M. Bosman, V.J. Keast, J.L. Garcia-Munoz, A.J. D'Alfonso, S.D. Findlay, L.J. Allen, Two-dimensional mapping of chemical information at atomic resolution, Physical Review Letters 99 (2007) 086102.
[139] D.A. Muller, L.F. Kourkoutis, M. Murfitt, J.H. Song, H.Y. Hwang, J. Silcox, N. Dellby, O.L. Krivanek, Atomic-scale chemical imaging of composition and bonding by aberration-corrected microscopy, Science 319 (2008) 1073–1076.
[140] M. Varela, M.P. Oxley, W. Luo, J. Tao, M. Watanabe, A.R. Lupini, S.T. Pantelides, S.J. Pennycook, Atomic-resolution imaging of oxidation states in manganites, Physical Review B 79 (2009) 085117.
[141] K. Suenaga, M. Koshino, Atom-by-atom spectroscopy at graphene edge, Nature 468 (2010) 1088–1090.
[142] T.J. Pennycook, M.P. Oxley, J. Garcia-Barriocanal, F.Y. Bruno, C. Leon, J. Santamaria, S.T. Pantelides, M. Varela, S.J. Pennycook, Seeing oxygen disorder in YSZ/$SrTiO_3$ colossal ionic conductor heterostructures using EELS, European Physical Journal Applied Physics 54 (2011) 33507.
[143] J. Garcia-Barriocanal, A. Rivera-Calzada, M. Varela, Z. Sefrioui, E. Iborra, C. Leon, S.J. Pennycook, J. Santamaria, Colossal ionic conductivity at interfaces of epitaxial ZrO_2:Y_2O_3/$SrTiO_3$ heterostructures, Science 321 (2008) 676–680.
[144] T.J. Pennycook, M.J. Beck, K. Varga, M. Varela, S.J. Pennycook, S.T. Pantelides, Origin of colossal ionic conductivity in oxide multilayers: interface induced sublattice disorder, Physical Review Letters 104 (2010) 115901.
[145] J. Gazquez, W.D. Luo, M.P. Oxley, M. Prange, M.A. Torija, M. Sharma, C. Leighton, S.T. Pantelides, S.J. Pennycook, M. Varela, Atomic-resolution imaging of spin-state superlattices in nanopockets within cobaltite thin films, Nano Letters 11 (2011) 973–976.
[146] R.F. Klie, J.C. Zheng, Y. Zhu, M. Varela, J. Wu, C. Leighton, Direct measurement of the low-temperature–spin-state transition in $LaCoO_3$, Physical Review Letters 99 (2007) 047203.
[147] O.L. Krivanek, G.J. Corbin, N. Dellby, B.F. Elston, R.J. Keyse, M.F. Murfitt, C.S. Own, Z.S. Szilagyi, J.W. Woodruff, An electron microscope for the aberration-corrected era, Ultramicroscopy 108 (2008) 179–195.
[148] B. Kabius, P. Hartel, M. Haider, H. Muller, S. Uhlemann, U. Loebau, J. Zach, H. Rose, First application of Cc-corrected imaging for high-resolution and energy-filtered TEM, Journal of Electron Microscopy 58 (2009) 147–155.
[149] M. Haider, P. Hartel, H. Müller, Current and future aberration correctors for the improvement of resolution in electron microscopy, Philosophical Transactions of the Royal Society of London A 367 (2009) 3665–3682.
[150] O.L. Krivanek, J.P. Ursin, N.J. Bacon, G.J. Corbin, N. Dellby, P. Hrncirik, M.F. Murfitt, C.S. Own, Z.S. Szilagyi, High-energy-resolution monochromator for aberration-corrected scanning transmission electron microscopy/electron energy-loss spectroscopy, Philosophical Transactions of the Royal Society of London A 367 (2009) 3683–3697.
[151] R. Leary, R. Brydson, Chromatic aberration correction: the next step in electron microscopy, in: P.W. Hawkes (Ed.), Advances in Imaging and Electron Physics, vol 165, 2011, pp. 73–130.
[152] C.T. Koch, W. Sigle, R. Höschen, M. Rühle, E. Essers, G. Benner, M. Matijevic, Sesam: Exploring the frontiers of electron microscopy, Microscopy and Microanalysis 12 (2006) 506–514.
[153] E. Essers, G. Benner, T. Mandler, S. Meyer, D. Mittmann, M. Schnell, R. Höschen, Energy resolution of an Omega-type monochromator and imaging properties of the MANDOLINE filter, Ultramicroscopy 110 (2010) 971–980.
[154] M.W. Chu, S.C. Liou, C.P. Chang, F.S. Choa, C.H. Chen, Emergent chemical mapping at atomic-column resolution by energy-dispersive X-ray spectroscopy in an aberration-corrected electron microscope, Physical Review Letters 104 (2010) 196101.
[155] A.J. D'Alfonso, B. Freitag, D. Klenov, L.J. Allen, Atomic-resolution chemical mapping using energy-dispersive X-ray spectroscopy, Physical Review B 81 (2010) 100101.
[156] L.J. Allen, S.D. Findlay, M.P. Oxley, C.J. Rossouw, Lattice-resolution contrast from a focused coherent electron probe. Part I, Ultramicroscopy 96 (2003) 47–63.
[157] L.F. Allard, W.C. Bigelow, M. Jose-Yacaman, D.P. Nackashi, J. Damiano, S.E. Mick, A new MEMS-based system for ultra-high-resolution imaging at elevated temperatures, Microscopy Research and Technique 72 (2009) 208–215.
[158] P.L. Gai, E.D. Boyes, Advances in atomic resolution in situ environmental transmission electron microscopy and 1 aberration corrected in situ electron microscopy, Microscopy Research and Technique 72 (2009) 153–164.
[159] A.A. Herzing, C.J. Kiely, A.F. Carley, P. Landon, G.J. Hutchings, Identification of active gold nanoclusters on iron oxide supports for CO oxidation, Science 321 (2008) 1331–1335.
[160] W. Zhou, E. Ross-Medgaarden, W. Knowles, M. Wong, I. Wachs, C. Kiely, Identification of active Zr–WO_x clusters on a ZrO_2 support for solid acid catalysts, Nature Chemistry 1 (2009) 722–728.
[161] D. Blom, W. Pyrz, T. Vogt, D. Buttrey, Aberration-corrected STEM investigation of the M2 phase of MoVNbTeO selective oxidation catalyst, Journal of Electron Microscopy 58 (2009) 193.
[162] S.N. Rashkeev, A.R. Lupini, S.H. Overbury, S.J. Pennycook, S.T. Pantelides, Role of the nanoscale in catalytic CO oxidation by supported Au and Pt nanostructures, Physical Review B 76 (2007) 035438.
[163] J.M. Thomas, Z. Saghi, P.L. Gai, Can a single atom serve as the active site in some heterogeneous catalysts? Topics in Catalysis 54 (2011) 588–594.
[164] S.J. Pennycook, Investigating the optical properties of dislocations by scanning transmission electron microscopy, Scanning 30 (2008) 287–298.